Applied Catalysis B: Environmental 176–177 (2015) 637–645

Contents lists available at ScienceDirect

Applied Catalysis B: Environmental

journal homepage: www.elsevier.com/locate/apcatb

Enhanced solar photodegradation of toxic pollutants by long-lived electrons in Ag–Ag_2O nanocomposites

Xuexiang Hu, Chun Hu*, Ran Wang

Key Laboratory of Drinking Water Science and Technology, Research Center for Eco-Environmental Sciences, Chinese Academy of Sciences, Beijing 10085, China

ARTICLE INFO

Article history:
Received 22 February 2015
Received in revised form 16 April 2015
Accepted 18 April 2015
Available online 20 April 2015

Keywords:
Ag–Ag_2O
Visible light photocatalysis
Nanocomposites
Toxic organic pollutant

ABSTRACT

Ag–Ag_2O was prepared by precipitation and thermal decomposition and characterized by X-ray diffraction and high-resolution transmission electron microscopy. A well-matched interfacial contact was formed between the Ag and Ag_2O nanoparticles (NPs) by drying Ag_2O at 70–100 °C. The nanocomposites exhibited a higher photoactivity and stability for the degradation and mineralization of toxic persistent organic pollutants compared to Ag_2O, which was demonstrated using 2-chlorophenol, 2,4-dichlorophenol and trichlorophenol under visible or near-infrared light irradiation and simulated solar irradiation. Based on electron storage and transient photocurrent, laser flash photolysis, and electron spin resonance analyses under a variety of experimental conditions, two sequential electron transfer processes were verified from photoexcited Ag_2O to Ag NPs to a thionine molecule or surface adsorbed oxygen as well as from water to the Ag_2O, resulting in $O_2^{\bullet-}$ and •OH. The maximum electron storage, the longest lifetime (757 μs) of photogenerated electrons and the strongest steady state photocurrent were observed for Ag–Ag_2O-70 °C, which resulted in the highest solar photoactivity. However, electron-hole recombination was dominant in the Ag–Ag_2O dried in other temperature ranges, leading to a much lower photoactivity. The results indicated that the interfacial contact with the metal/semiconductor played a key role in charge separation and migration, which improved their photocatalytic efficiency. These results will allow for the application of narrow bandgap semiconductors that can harvest the full spectrum of sunlight to be employed in photocatalysis and photovoltaic fuel cells.

1. Introduction

The efficiency of solar conversion in photocatalytic detoxification and photovoltaic fuel cells depends on four processes: light absorption, charge separation, charge migration, and surface reactions [1,2]. Semiconductors used in photovoltaic and photocatalytic devices have a low solar energy conversion efficiency due to limitations in one or more of these four processes. For example, widely applied semiconductors, such as titanium (TiO_2) and perovskite ($La_2Ti_2O_7$), only absorb ultraviolet light [3,4], which accounts for less than 5% of the total solar radiation [5]. To increase the light absorption of sunlight, extensive efforts have focused on achieving visible-light photocatalysts including the use of metal or nonmetal–doped TiO_2 [3,6–9], coupled semiconductor [10–12], and plasmonic photocatalysts [13–15]. However, some narrow bandgap semiconductors (i.e., 1.4–1.5 eV), which are ideal for harvesting the full spectrum of sunlight [16], do not exhibit maximum energy conversion efficiency in photocatalysis and photovoltaic fuel cells due to the higher recombination rate of the photogenerated charge carriers and photocorrosion [17] (e.g., CdS [18] and CdSe [19]). The effectiveness of solar-driven photoconversion processes is dictated to a great extent by both the absorption of light and the suppression of the rapid combination of photogenerated electrons and holes. Surface plasmon effects and core–shell structures have been used to prolong the lifetimes of charged carriers and prevent photocorrosion, as shown in the preparation of the Ag/AgCl [20] and Cu_2O@TiO_2 [21] hybrid structures.

The metal-semiconductor interface provides a unique pathway for capturing, storing and discharging photogenerated electrons [22–24]. The presence of metal nanoparticles may provide efficient charge separation and migration, enhancing the surface oxidation and reduction reactions to facilitate the activity and stability of photocatalysts. Ag_2O is a narrow bandgap material with a band gap of 1.3 eV [25], and this material has been widely used in many industrial products [26,27]. Recently, some researchers reported that Ag_2O could act as an active photocatalyst and exhibited self-stability with the formation of a Ag–Ag_2O structure during the photocatalytic reaction [28]. However, the exact mechanism of this

* Corresponding author. Tel.: +86 10 62849171; fax: +86 10 62923541.
E-mail address: huchun@mail.rcees.ac.cn (C. Hu).

http://dx.doi.org/10.1016/j.apcatb.2015.04.040
0926-3373/

enhanced photostability and photoactivity has not yet been elucidated.

In this study, a series of Ag–Ag_2O nanocomposite photocatalysts were prepared using a simple precipitation and thermal decomposition method. Organic compounds, especially phenolic compounds, are considered to be hazardous waste that is highly toxic and difficult to biologically degrade, which has resulted in rigid limits on the acceptable level of phenol in the environment. Several ubiquitous water polluting phenolic compounds (i.e., 2-chlorophenol (2-CP), 2, 4-dichlorophenol (2, 4-DCP) and trichlorophenol (TCP)) were selected to evaluate the activity and properties of the catalysts under visible or near-infrared light irradiation and simulated solar irradiation. The lifetime of the charge carrier in Ag_2O was greatly increased because it was further loaded with Ag nanocomposites (NPs), which significantly enhanced the photocatalytic activity for the degradation and mineralization of the tested phenolic compounds. The electron transfer processes between photoexcited Ag_2O and Ag were investigated by probing the electron storage, transient photocurrent, laser flash photolysis, and electron spin resonance (ESR).

2. Experimental

2.1. Chemicals materials

The 5-tert-butoxycarbonyl 5-methyl-1-pyrroline N-oxide (BMPO) reagent, which was used as the spin trapping agent in the ESR studies, was purchased from the Bioanalytical Lab (Sarasota, FL). Superoxide dismutase (SOD) was purchased from the Sigma Chemical Co. All of the other chemicals used were analytical grade, purchased from the Beijing Chemical Co., and used without further purification.

2.2. Preparation of catalysts

The Ag–Ag_2O samples was synthesized through precipitation and thermal decomposition method. 0.58 g of $AgNO_3$ were dissolved in 50 mL of deionized water, and then, a 2 M aqueous NaOH solution were added dropwise into the aqueous solution to achieve a pH of 14. The $AgNO_3$ reacts with NaOH to form AgOH. The intermdiated AgOH is thermodynamically unstable, and ultimately dissociated to form Ag_2O nuclei. Next, the suspension was stirred overnight to ensure complete reaction and the Ag_2O nuclei concentration enlarges. Finally, the obtain precipitate was washed thoroughly with deionized water and was dried in air at 40–150 °C to thermally decomposed to Ag–Ag_2O composites. For comparison, the pure Ag_2O nanoparticels were also synthesized in the same way except for the use of vacuum freeze-drying.

2.3. Characterization

X-ray diffraction (XRD) patterns (XDS-2000 diffractometer; Scintag, CA) and UV–vis-NIR diffuse reflectance spectra (Hitachi UH4150) were obtained for the samples. High-resolution transmission electron microscopy (HRTEM) images were recorded using a JEOL-2010 TEM with an acceleration voltage of 200 kV. The ESR spectra were obtained using a Bruker model A300-10/12 electron paramagnetic resonance spectrometer. The photocurrent from the various samples was measured in a basic electrochemical system with a three-electrode electrochemical cell equipped with a photocatalyst photoanode (prepared by dip-coating and drying in air) and a platinum wire cathode in a 0.1 M Na_2SO_4 solution. The reference electrode was a saturated calomel electrode. A constant voltage of 0.35 V was applied. The responding photocurrent was recorded by an electrochemical workstation (CHI 660D, Chenhua Co., China). Nanosecond laser flash photolysis using a 355 nm laser

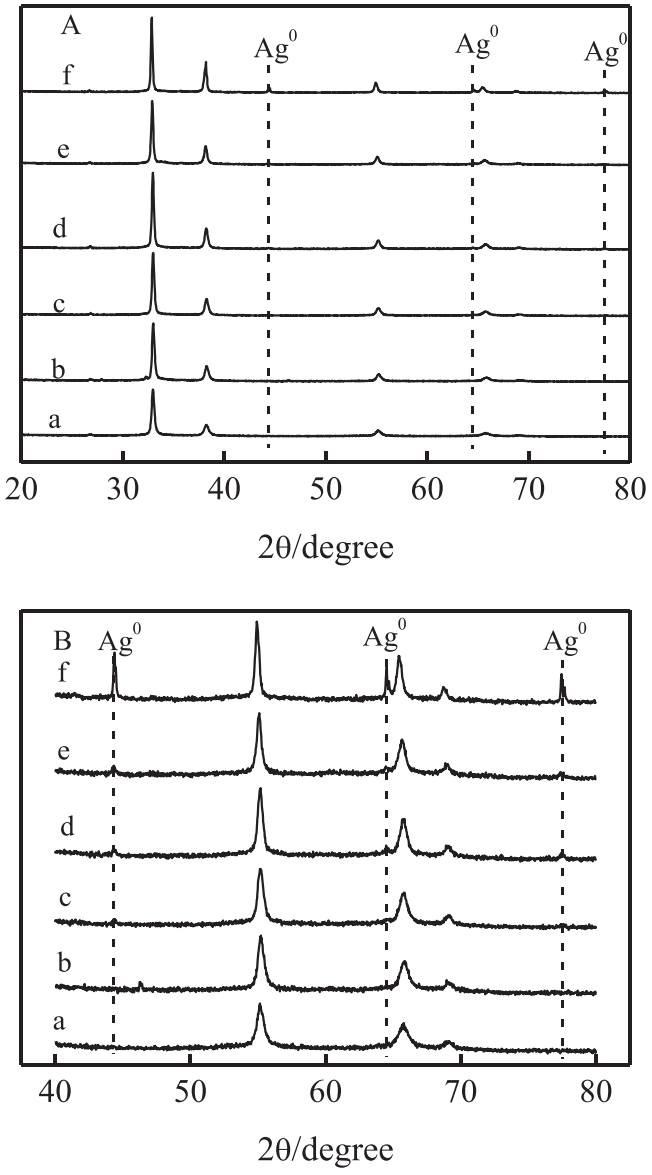

Fig. 1. XRD patterns (A) and expansion of diffraction data (B) of different nanocrystals: (a) Ag_2O, (b) Ag–Ag_2O-40 °C, (c) Ag–Ag_2O-70 °C, (d) Ag–Ag_2O-100 °C, (e) Ag–Ag_2O-120 °C, (f) Ag–Ag_2O-150 °C.

was carried out with a LP920 type measurement system (Edinburgh Instruments) at ambient temperature. The experiments were performed under an air-saturated or N_2-saturated aqueous suspension. The decay curve was captured with a 100 MHz TDS3012B oscilloscope by 2000-channel digitals.

2.4. Photocatalytic degradation of chlorophenol compounds under visible and near-infrared light irradiation

Photocatalytic experiments were performed in a beaker with aqueous suspensions of chlorophenol (60 mL, 10 mg L^{-1}) and 50 mg of the catalyst powder. The light source was a 150 W Xe arc lamp equipped with a wavelength cutoff filter for $\lambda > 420$ nm, 600 nm, and 800 nm focused on the beaker. Prior to irradiation, the suspensions were magnetically stirred in the dark for 30 min to establish adsorption/desorption equilibrium between the pollutants and the surface of the photocatalyst under room air equilibrated conditions. The concentration of each chlorophenol suspension was measured using high-performance liquid chromatography (1200 series; Agilent) with an Eclipse XDB-C18 column (5 μm, 4.6 × 150 mm;

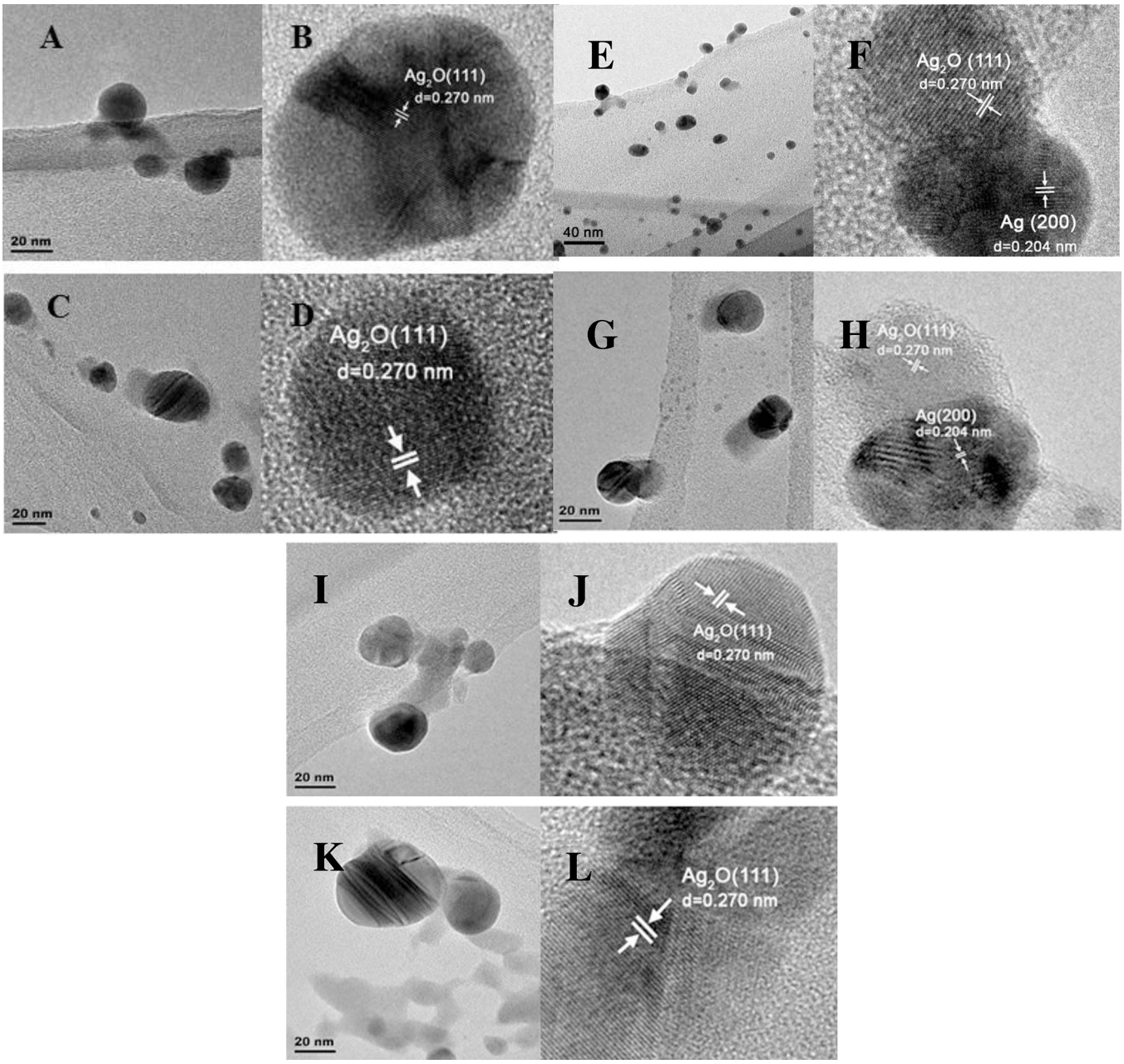

Fig. 2. HRTEM images of samples: (A and B) Ag_2O, (C and D) Ag–Ag_2O-40 °C, (E and F) Ag–Ag_2O-70 °C, (G and H) Ag–Ag_2O-100 °C, (I and J) Ag–Ag_2O-120 °C, (K and L) Ag–Ag_2O-150 °C.

Agilent). The total organic carbon (TOC) of each solution was measured with a TOC analyzer (TOC-VCPH, Shimadzu). In the recycling experiments, the photocatalyst was filtered and washed with deionized water prior to being redispersed in the 2-CP solution for another cycle.

2.5. Estimation of electrons stored in the Ag–Ag_2O samples

The electrons stored in the Ag–Ag_2O and Ag_2O nanoparticles were estimated with an electron acceptor thionine (TH). The TH dye, which has an absorption at 600 nm ($\epsilon = 60000\ M^{-1}\ cm^{-1}$), undergoes a two-step reduction process to form a colorless product, leuco dye (TH^{2-}), with no absorption in the visible region. Therefore, the disappearance of one TH molecule represents the transfer of two electrons [29]. The Ag–Ag_2O or Ag_2O suspension was subjected to visible irradiation for different time periods under a N_2 atmosphere. After the visible irradiation was terminated, a known amount of deaerated TH solution was added. After reacting for 5 min, the dispersion were pipetted and centrifuged at 8000 rpm for 5 min. The concentration of TH was monitored using UV–vis spectroscopy at 600 nm. Due to absorption on the surface of photocatalyst, the concentration of TH in the suspension after 5 min without pre-irradiation was used as the control. The net reduction of TH was measured, and then, the number of electrons stored in these particles was calculated.

3. Results and discussion

3.1. Characterization of photocatalysts

The XRD patterns of samples dried at different temperatures are shown in Fig. 1. All of the samples exhibited diffraction peaks

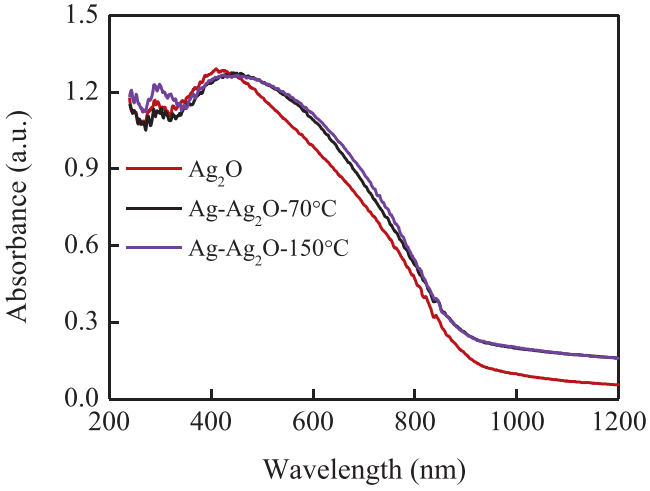

Fig. 3. Diffuse reflectance UV–vis spectra of different samples.

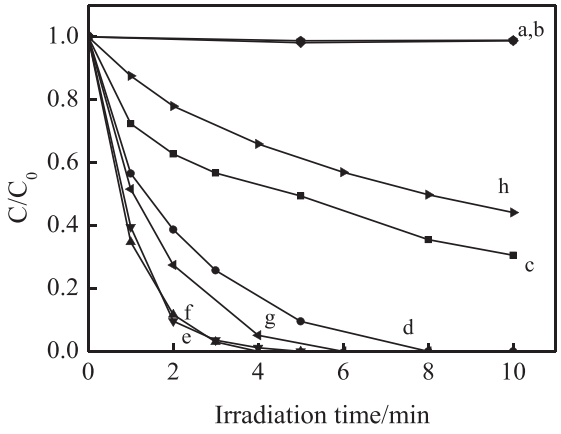

Fig. 4. Temporal course of photodegradation of 2-CP (10 mg L^{-1}; 60 mL) in aqueous dispersions (containing catalyst: 0.8 g L^{-1}) under visible light irradiation (λ > 420 nm): (a) no catalyst, (b) Ag–Ag_2O-70 °C in dark, (c) Ag_2O, (d) Ag–Ag_2O-40 °C, (e) Ag–Ag_2O-70 °C, (f) Ag–Ag_2O-100 °C, (g) Ag–Ag_2O-120 °C, (f) Ag–Ag_2O-150 °C.

at 26.82°, 32.97°, 38.17°, 55.26°, and 65.76°, which were primarily indexed as cubic Ag_2O (JCPDS card No. 41-1104). In addition, the diffraction peaks located at 44.4° and 64.4° were assigned to metallic Ag (JCPDS card No. 87-597) in these samples dried at higher than 40 °C, and the intensities of these peaks increased with increasing temperature, suggesting the coexistence of Ag_2O and metallic Ag in these samples. The appearance of metallic Ag indicated the existence of a slow thermal decomposition of Ag_2O precipitate during the drying process and the decomposition reaction was sped up by the temperature increase, which also was proved by the previous study [30]. The TEM image of Ag_2O (Fig. 2A) indicated that the nanoparticles were uniform, approximately 7–20 nm in size, and highly crystalline. The lattice fringes at 0.270 nm corresponded to the (1 1 1) plane of Ag_2O in Fig. 2B. Ag–Ag_2O dried at 40–100 °C possessed similar particle size ranges from 7 to 22 nm, and the particle sizes were 16–27 nm and 16–52 nm for Ag–Ag_2O-120 °C and Ag–Ag_2O-150 °C (Fig. 2). In Ag–Ag_2O-70 °C, two lattice fringe spaces at 0.204 nm and 0.270 nm were observed corresponding to the (2 0 0) plane of metallic Ag and the (1 1 1) plane of Ag_2O for the Ag–Ag_2O-70 °C sample (Fig. 2F). The results confirmed that the heterojunction structure was formed with good interfacial contact between Ag_2O and Ag NPs, which is beneficial to interfacial charge carrier transfer. The same heterojunction structure of Ag–Ag_2O was also observed in Ag–Ag_2O-100 °C (Fig. 2H). In contrast, the uniform contact of Ag and Ag_2O NPs was not observed in the Ag–Ag_2O-40 °C, Ag–Ag_2O-120 °C and Ag–Ag_2O-150 °C samples, in which the lattice fringes of Ag_2O were predominantly observed. The optical properties of different samples are shown in Fig. 3, and all of the samples exhibit strong absorption of ultraviolet to near-infrared light. Therefore, these samples possess the potential to enhance solar-driven photocatalytic activity.

3.2. Photodegradation of pollutants under visible and near-infrared light irradiation

The photocatalytic activities of the different photocatalysts were evaluated based on the degradation of 2-CP under visible light irradiation (λ > 420 nm) after the adsorption of 2-CP onto the photocatalyst had reached equilibrium in the dark (Fig. 4). No significant adsorption of 2-CP was observed on these photocatalysts in the dark. Ag–Ag_2O-70 °C and Ag–Ag_2O-100 °C exhibited a similar photoactivity, and 2-CP was completely degraded within 4 min in the two photocatalyst suspensions under visible light irradiation (λ > 420 nm). However, only 35% of 2-CP was removed in the Ag_2O suspensions under identical conditions, and the rate of 2-CP photodegradation on Ag–Ag_2O-70 °C was 8.63 times faster than that on Ag_2O (Table 1). The activity of Ag–Ag_2O dried at 40 °C and 120 °C decreased, and the sample dried at 150 °C exhibited the lowest activity, which was due to the lack of heterojunction structure formation in the sample. Therefore, optimal matching of Ag and Ag_2O was achieved by drying Ag_2O in the temperature range of 70–100 °C. Under irradiation of light at λ > 600 nm, the complete degradation of 2-CP in Ag–Ag_2O-70 °C occurred within 40 min (Fig. 5). However, using the Ag_2O suspension, the complete degradation of 2-CP required 70 min. In addition, at λ > 800 nm, 82% of 2-CP was removed by Ag–Ag_2O-70 °C within 90 min, and only 28% of 2-CP was removed by Ag_2O under the same conditions (Fig. 5). Because the surface plasmon absorption of Ag NPs

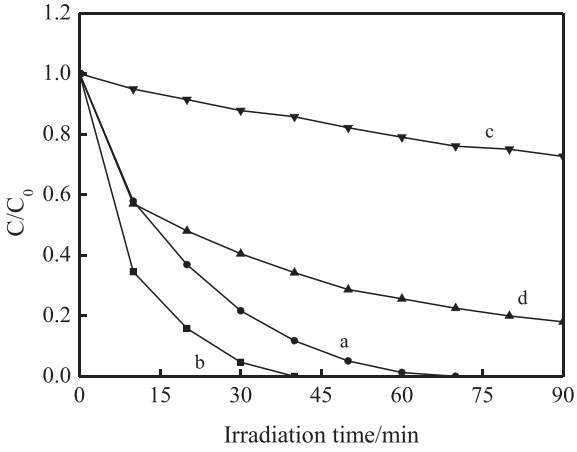

Fig. 5. Temporal course of photodegradation of 2-CP (10 mg L^{-1}; 60 mL) in aqueous dispersions (containing catalyst: 0.8 g L^{-1}): (a) Ag_2O, (b) Ag–Ag_2O-70 °C under light irradiation of λ > 600 nm; and (c) Ag_2O, (d) Ag–Ag_2O-70 °C under light irradiation of λ > 800 nm.

Table 1
The apparent reaction rate constant (*k*) of 2-CP degradation in different photocatalysts suspensions under visible light irradiation (λ > 420 nm).

Samples	k (min^{-1})	r^2
Ag_2O	0.1311	0.8719
Ag–Ag_2O-40 °C	0.4684	0.9959
Ag–Ag_2O-70 °C	1.1315	0.9955
Ag–Ag_2O-100 °C	1.1109	0.9963
Ag–Ag_2O-120 °C	0.7217	0.993
Ag–Ag_2O-150 °C	0.0879	0.9698

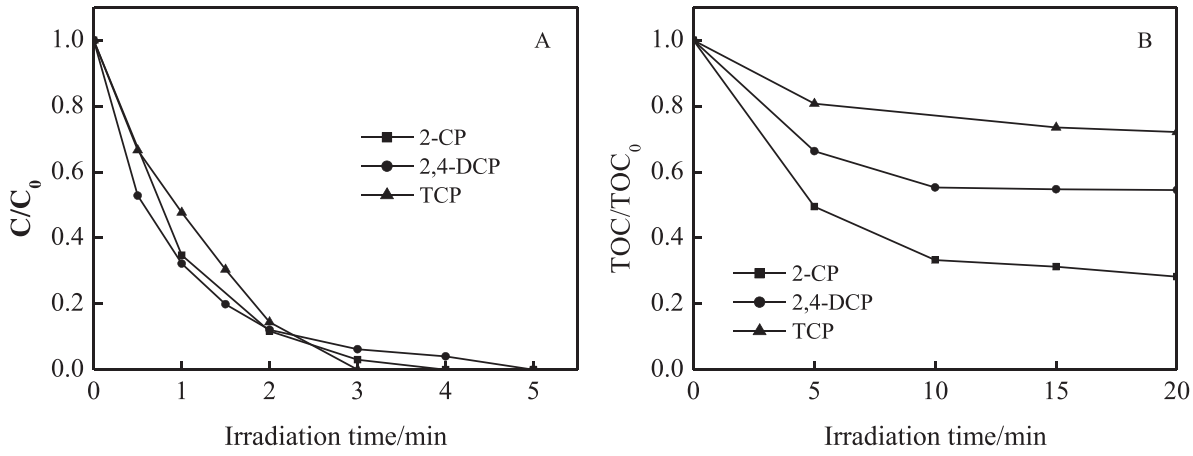

Fig. 6. Photodegradation (A) and mineralization (B) different pollutants in aqueous dispersions of Ag–Ag_2O-70 °C under visible light λ > 420 nm.

occurs at approximately 400–600 nm [31], the results confirmed that the photocatalytic activity of Ag_2O was greatly enhanced by the hybridization of metallic Ag enhancing the electron–hole separation due to electron trapping. In addition, 2, 4-DCP and TCP were completely degraded within 5 and 3 min, respectively, in a Ag–Ag_2O-70 °C suspension under visible light irradiation (Fig. 6A). 71.8%, 45.5% and 27.9% of the TOC were removed after 20 min for 2-CP, 2, 4-DCP, and TCP, respectively (Fig. 6B). Under simulated solar light (λ > 330 nm), 2-CP was completely removed in the Ag–Ag_2O suspension within 3 min, and only approximately 3.5% of 2-CP was degraded in the P25 TiO_2 suspension in the same amount of time (Fig. 7). The rate of the former was 150 times faster than the latter. In addition, the photocatalytic activity of Ag–Ag_2O-70 °C did not markedly decrease after 9 successive cycles of degradation testing under visible irradiation (Fig. 8). The Ag–Ag_2O nanocrystals exhibited substantial activity and stability in the photocatalytic process with sunlight.

3.3. Electron storage and charge carrier lifetime

When the metal and semiconductor are in contact, the free electrons will transfer between the metal and the semiconductor due to the work function difference [32]. Fig. S1 shows the energy band diagrams of Ag and Ag_2O contacts. In dark, as the work function of the Ag NPs (4.3 eV)[33] is lower than that of Ag_2O (i.e., 5.3 eV) [34], electrons will flow from Ag NPs to Ag_2O until thermodynamic equilibrium is established, resulting in an accumulation layer and the edges bend downward toward the interface of Ag–Ag_2O (shown in Fig. S1) [32]. There will be an inner electric field in the interface between Ag_2O and Ag, leading to a negatively charged region in the Ag_2O part. After the illumination of visible light, the photoinduced electrons in the CB of Ag_2O would move to the positively charged Ag NPs by the drive of inner field, while the holes will keep in the VB of Ag_2O. Therefore, the photogenerated carriers can be efficiently separated. A fraction of the electrons transferred during visible light irradiation should remain stored in the Ag NPs of the nanocomposites in a N_2-saturated aqueous solution after the irradiation is terminated. These electrons can be discharged by reducing the TH dye to produce a two-electron reduction product [29]. Therefore, the disappearance of one TH molecule represents a transfer of two electrons, which has been used to determine the quantitative transfer of electrons from the semiconductor to the metal particles. The results in Fig. 9 indicate that the number of stored electrons increased with increasing irradiation time in different Ag–Ag_2O composite suspensions. No significant electron storage was detected in the Ag_2O suspension. A maximum electron storage (16 μM) was obtained at an irradiation time of 6 min for Ag–Ag_2O-70 °C, and the maximum amount of stored electrons was 6.5 μM and 10 μM for Ag–Ag_2O-40 °C at 6 min of irradiation and Ag–Ag_2O-150 °C at 8 min, respectively. The capacity for electron storage increased as the size of the Ag NPs increased. This capacity reached a maximum at a Ag NP size of 7–22 nm and then decreased at sizes >22 nm. The results indicated that the electron storage

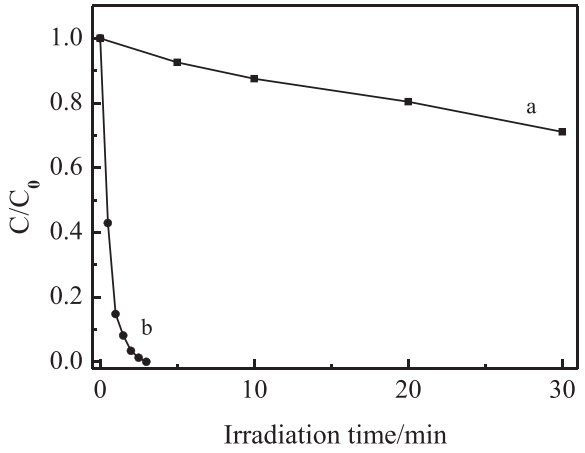

Fig. 7. The photodegradation of 2-CP (10 mg L^{-1}, 60 mL) in aqueous dispersions (containing catalyst: 0.8 g L^{-1}) under simulated solar light (λ > 330 nm): (a) P25 TiO_2, (b) Ag–Ag_2O-70 °C.

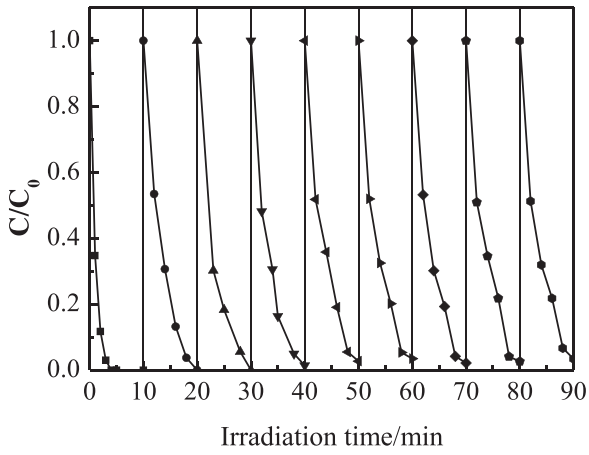

Fig. 8. Cycling tests of visible photocatalytic activity (2-CP decomposition) of the Ag–Ag_2O-70 °C nanocomposite under visible light λ > 420 nm.

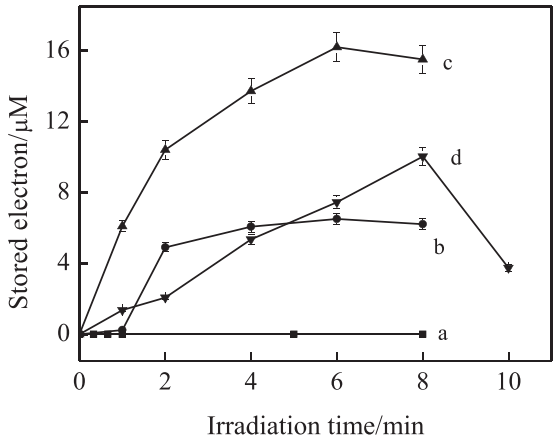

Fig. 9. Dependence of number stored electrons on the time of visible light irradiation (λ > 420 nm) in different photocatalysts suspension: (a) Ag_2O, (b) Ag–Ag_2O-40 °C, (c) Ag–Ag_2O-70 °C, (d) Ag–Ag_2O-150 °C.

depended on the size of the Ag NPs in the Ag–Ag_2O suspensions. The larger Ag NPs would become the trapping center for photogenerated electrons and holes, leading to less electron storage, and the smaller one would trap fewer electrons. After this maximum storage was attained, electron-hole recombination dominated in the composites. Therefore, the electron storage enhanced photogenerated electron-hole separation, inhibiting recombination and prolonging the charge carrier lifetime. The transient absorption spectra, which were recorded after 355 nm laser pulse excitation of air-saturated or N_2-saturated catalyst suspensions, are shown in Fig. 10. The N_2-saturated aqueous dispersion of Ag_2O exhibited a broad absorption in the 300–700 nm region, and a much weaker absorption was observed in the air-saturated aqueous dispersion of Ag_2O. This result indicated that the photoexcited electrons were rapidly trapped by the surface-adsorbed oxygen on Ag_2O, leading to fewer electrons. Therefore, the absorption band was ascribed to the transitions of photoexcited electrons based on our results and those from previous studies [31,35]. Therefore, the air-saturated aqueous dispersion of Ag–Ag_2O-70 °C exhibited photoexcited electron transition in the 300–800 nm region. The transitions of the photoexcited electrons became weaker and exhibited absorption peaks at approximately 390 nm and 625 nm, which was due to the electron storage of the Ag NPs (Fig. 10). The same phenomena were observed for the Ag–Ag_2O-40 °C samples under identical conditions. However, the Ag–Ag_2O-150 °C sample exhibited a transition absorption similar to Ag_2O in an air-saturated aqueous suspension. However, no absorption was observed for the N_2-saturated aqueous suspension, indicating primarily electron-hole recombination. In addition, the decay kinetics curve of the photogenerated electron was obtained by the transient absorption recorded at 400 nm (Fig. 11). The experimental curve was fit according to $\Delta OD = A_1 \times \exp(-t/\tau_1) + A_2 \times \exp(-t/\tau_2)$, where τ_1 and τ_2 refer to the band edge lifetime and trapping or defect states, respectively (Table 2). The average lifetime (τ_{av}) was calculated using the following equation: $\tau_{av} = (A_1\tau_1 + A_2\tau_2)/(A_1 + A_2)$ [36], where A_1 and A_2 are the amplitude of the band edge exciton and trapping state emission, respectively. The Ag–Ag_2O-70 °C sample exhibited the longest τ_1 (49.17 μs) and an average lifetime of 757 μs, which was in agreement with the best electron storage and photoactivity. The Ag–Ag_2O-40 °C and Ag–Ag_2O-150 °C samples exhibited an average

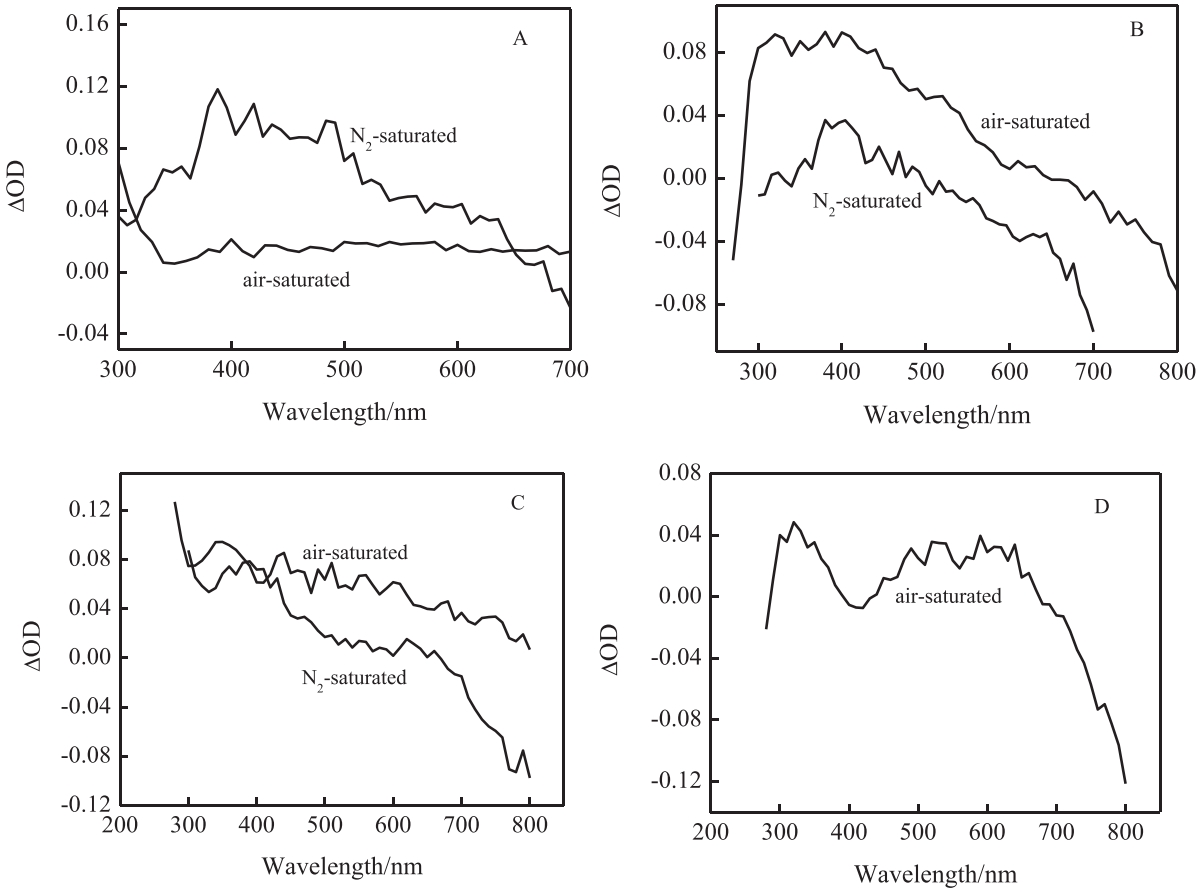

Fig. 10. Transient absorption spectra of different samples in air-saturated and N_2-saturated aqueous solution: (A) Ag_2O, (B) Ag–Ag_2O-40 °C, (C) Ag–Ag_2O-70 °C, (D) Ag–Ag_2O-150 °C.

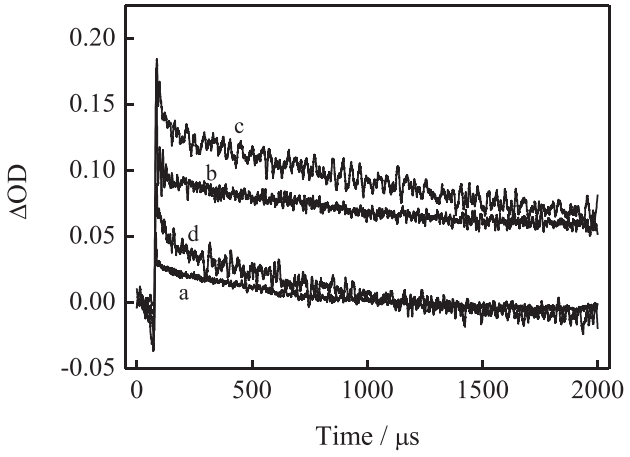

Fig. 11. Transient decay observed at 400 nm of different air-saturated catalysts suspension following 355 nm laser excitation. (a) Ag_2O, (b) Ag–Ag_2O-40 °C, (c) Ag–Ag_2O-70 °C, (d) Ag–Ag_2O-150 °C.

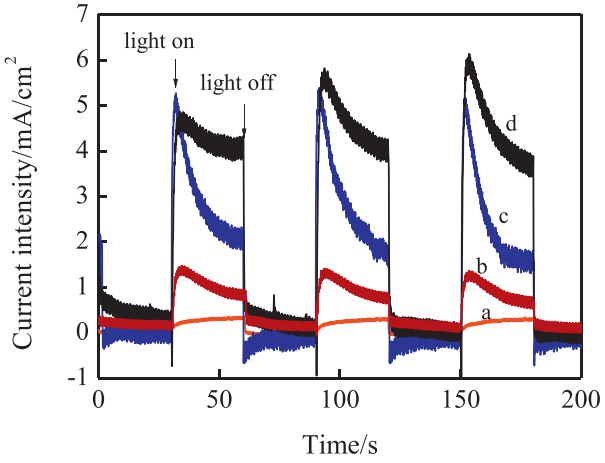

Fig. 12. The transient photocurrent response of the Ag_2O and Ag–Ag_2O photoelectrodes under visible light irradiation (λ > 420 nm) in 0.1 M Na_2SO_4 solutions: (a) Ag_2O, (b) Ag–Ag_2O-40 °C, (c)Ag–Ag_2O-70 °C, (d)Ag–Ag_2O-150 °C.

Table 2
Summary of transient decays data of different photocatalysts.

Sample	τ_1 (μs)	τ_2 (μs)	τ_{av} (μs)
Ag_2O	15.57	634.3	550
Ag–Ag_2O-40 °C	3.16	893.9	257
Ag–Ag_2O-70 °C	49.17	850.0	757
Ag–Ag_2O-150 °C	6.81	670.8	217

lifetime of 257 μs and 217 μs, respectively, which was not consistent with the electron storage due to the shorter lifetime to band edge lifetime (τ_1). A relatively longer average lifetime (550 μs) was observed for Ag_2O due to a longer lifetime of 15.57 μs to the band edge. In addition, Ag_2O exhibited the shortest τ_2 lifetime. These results confirmed that long-lived photogenerated electrons (757 μs) could be achieved by the electron capture on the Ag NPs during light irradiation.

3.4. Charge migration and surface reaction

Because charge separation and migration have to compete with the recombination of electrons and holes, which could occur in the bulk or on the surface of Ag_2O, not all long-lived charge carriers can contribute to the photocatalytic reaction. Therefore, the transient surface photocurrent responses of different photocatalysts were recorded for several on-off cycles of irradiation (Fig. 12). Upon irradiation, due to the fast generation and separation of the electron-hole pairs, the highest photocurrent density spike (J_{in}, 5.31 mA cm^{-2}) [37] formed on the surface of the Ag–Ag_2O-70 °C sample, and the second highest one (5.15 mA cm^{-2}) appeared on the surface of the Ag–Ag_2O-40 °C sample. In addition, Ag–Ag_2O-150 °C and Ag_2O exhibited a much lower J_{in}, indicating that more recombination of electrons with holes occurred. The reasonably sizes Ag NPs could enhance the separation of the electron-hole pairs. Subsequently, J_{in} decreased until equilibrium was achieved. This phenomenon may be due to the unavoidable recombination of electrons with holes during electron migration. A steady state photocurrent density (J_{st}) [37] was observed when the generation rate and the recombination rate reached equilibrium. J_{st} was 3.74 mA cm^{-2} for Ag–Ag_2O-70 °C, which was 1.84-fold higher than that for Ag–Ag_2O-40 °C (2 mA cm^{-2}). 29.6% of the J_{in} electrons recombined with holes in Ag–Ag_2O-70 °C, and 61.6% of the J_{in} electrons recombined with holes during charge migration to the surface of the photocatalysts in the Ag–Ag_2O-40 °C sample. In addition, J_{st} of Ag–Ag_2O-150 °C (0.52 mA cm^{-2}) was nearly the same as that of Ag_2O due to higher recombination of electrons with holes even though Ag_2O-Ag-150 °C possessed a higher J_{in} (1.13 mA cm^{-2}) than Ag_2O (0.22 mA cm^{-2}). After irradiation was terminated, the separated electron/hole pairs immediately recombined, and the J_{st} exhibited a slower decay in Ag–Ag_2O-70 °C. However, J_{st} rapidly decreased to nearly zero in the other Ag–Ag_2O and Ag_2O photocatalysts. The results further confirmed that the reasonable size of the Ag NPs and good interfacial contact between Ag_2O and the Ag NPs play an important role in charge storage, charge migration, and charge recombination to improve the photoelectrochemical properties of a mesoscopic semiconductor for photocatalytic detoxification and photovoltaic fuel cells. ESR with BMPO was used to study the surface reactions of the surface photogenerated electrons and holes with adsorbed oxygen and water molecules, respectively. The characterization peaks of BMPO- $O_2^{\bullet-}$ were observed in all of the photocatalyst suspensions with visible light irradiation (Fig. 13A). No such signals were detected in the dark. The Ag–Ag_2O-70 °C sample exhibited the strongest peak intensities, and the Ag_2O sample exhibited the weakest ones, which is consistent with the surface photocurrent data indicating that there are more electrons available to participate in the surface reaction on the Ag–Ag_2O-70 °C sample. Similarly, four characteristic peaks for BMPO- •OH were observed in all of the photocatalyst suspensions (Fig. 13B). No such signals were detected in the dark. The strongest peak intensities were observed for the Ag–Ag_2O-70 °C suspension, and the weakest ones were observed in the Ag_2O suspension. The surface photogenerated hole reacted with a surface adsorbed water and hydroxyl group to form •OH [38]. However, during photocatalysis, $O_2^{\bullet-}$could also be transformed to •OH by double-electron reduction from a photogenerated electron [39]. Therefore, SOD was added to the Ag–Ag_2O-70 °C suspension to quench $O_2^{\bullet-}$ and prevent its conversion to •OH under identical conditions. No significant changes in the intensities of the BMPO- •OH peaks were observed (Fig. 14), indicating that the •OH that formed predominantly came from the reaction of the surface hole with the adsorbed water/hydroxyl, which suggested that more holes participate in the surface reaction on Ag–Ag_2O-70 °C. These results further demonstrate that the heterojunction structure with reasonably sized Ag NPs and good interfacial contact on Ag–Ag_2O-70 °C can more effectively promote charge separation and migration, inhibiting recombination. Therefore, more long-lived photogenerated charges contributed to the photocatalytic degradation of pollutants. The photocorrosion of the photocatalyst itself will occur if the photogenerated charge carriers do not transfer to the surface and are not quickly removed via surface reactions. The photostability of Ag–Ag_2O predominantly contributed to the Ag–Ag_2O interface to achieve rapid charge

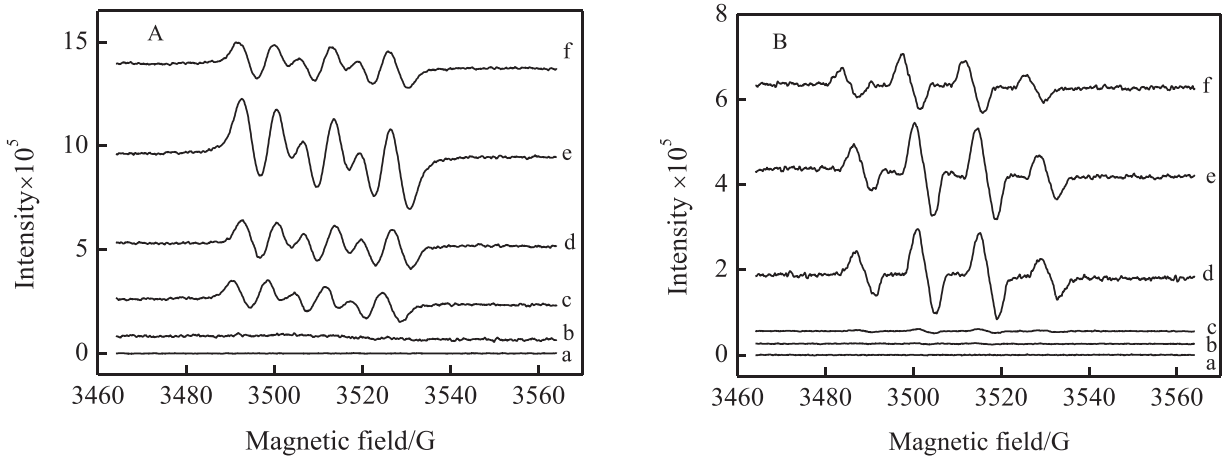

Fig. 13. ESR signal in methanol dispersion (for BMPO- $O_2^{\bullet-}$, (A) and aqueous dispersion (for BMPO- •OH, (B) under visible light irradiation ($\lambda > 420$ nm): (a) BMPO control, (b) Ag–Ag_2O-70 °C in dark, (c) Ag_2O, (d) Ag–Ag_2O-40 °C, (e) Ag–Ag_2O-70 °C, (f) Ag–Ag_2O-150 °C.

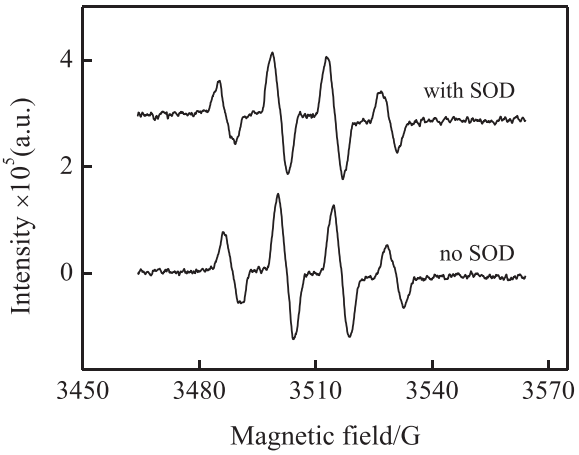

Fig. 14. Effect of SOD addition on the ESR signal of BMPO- •OH in Ag–Ag_2O-70 °C suspension under visible light irradiation ($\lambda > 420$ nm).

separation, migration and surface reactions. Therefore, both the activity and stability of the photocatalyst have the same requirements for the electron-transfer process.

4. Conclusions

Good interfacial contact of the heterojunction structure was formed between Ag_2O and the Ag NPs by drying Ag_2O in the temperature range of 70–100 °C. The nanocomposites exhibit enhanced photoactivity and stability for the degradation and mineralization of 2-CP, 2,4-DCP, and TCP relative to Ag_2O under visible, near-infrared light and simulated solar irradiation. Two sequential electron transfer processes were observed from the photoexcited Ag_2O to the Ag NPs to the TH molecule or surface adsorbed oxygen as well as from water to Ag_2O, resulting in $O_2^{\bullet-}$and •OH. The maximum electron storage, longest electron lifetime and strongest steady state photocurrent were observed for Ag–Ag_2O-70 °C, which resulted in the highest solar photoactivity. In contrast, the same parameters became much weaker, and electron-hole recombination was dominant in the Ag–Ag_2O sample dried in other temperature ranges, which resulted in a much lower photoactivity. The results indicated that the interfacial contact of the metal/semiconductor played a key role in charge separation and migration to improve their photocatalytic efficiency. These results will allow for the application of narrow bandgap semiconductors that can harvest the full spectrum of sunlight to be employed in photocatalysis and photovoltaic fuel cells.

Acknowledgments

This work is supported by the NSFC (Nos. 21125731 and 51221892). We wish to thank Dr. Wenhua Leng (Department of Chemistry, Zhejiang University) for valuable discussions regarding the laser flash photolysis studies.

Appendix A. Supplementary data

Supplementary data associated with this article can be found, in the online version, at http://dx.doi.org/10.1016/j.apcatb.2015.04.040.

References

[1] N. Wu, J. Wang, D.N. Tafen, H. Wang, J.-G. Zheng, J.P. Lewis, X. Liu, S.S. Leonard, A. Manivannan, J. Am. Chem. Soc. 132 (2010) 6679–6685.
[2] S.K. Cushing, J. Li, F. Meng, T.R. Senty, S. Suri, M. Zhi, M. Li, A.D. Bristow, N. Wu, J. Am. Chem. Soc. 134 (2012) 15033–15041.
[3] R. Asahi, T. Morikawa, T. Ohwaki, K. Aoki, Y. Taga, Science 293 (2001) 269–271.
[4] P. Liu, J. Nisar, B. Sa, B. Pathak, R. Ahuja, J. Phys. Chem. C 117 (2013) 13845–13852.
[5] X. Chen, S. Shen, L. Guo, S.S. Mao, Chem. Rev. 110 (2010) 6503–6570.
[6] S.U.M. Khan, M. Al-Shahry, W.B. Ingler, Science 297 (2002) 2243–2245.
[7] H. Yamashita, M. Harada, J. Misaka, M. Takeuchi, K. Ikeue, M. Anpo, J. Photochem. Photobiol. A: Chem. 148 (2002) 257–261.
[8] S. Yin, B. Liu, P. Zhang, T. Morikawa, K. Yamanaka, T. Sato, J. Phys. Chem. C 112 (2008) 12425–12431.
[9] X. Pan, M. Yang, X. Fu, N. Zhang, Y. Xu, Nanoscale 5 (2013) 3601–3614.
[10] L. Ge, C. Han, X. Xiao, L. Guo, Int. J. Hydrogen Energy 38 (2013) 6960–6969.
[11] M. yang, N. Zhang, M. Pagliaro, Y. Xu, Chem. Soc. Rev. 43 (2014) 8240–8254.
[12] C. Han, L. Ge, C. Chen, Y. Li, X. Xiao, Y. Zhang, L. Guo, Appl. Catal. B 147 (2014) 546–553.
[13] C. Hu, T. Peng, X. Hu, Y. Nie, X. Zhou, J. Qu, H. He, J. Am. Chem. Soc. 132 (2009) 857–862.
[14] X. Xiao, L. Ge, C. Han, Y. Li, Z. Zhao, Y. Xin, S. Fang, L. Wu, P. Qiu, Appl Catal. B. 163 (2015) 564–572.
[15] R. Jiang, B. Li, C. Fang, J. Wang, Adv. Mater. 26 (2014) 5274–5309.
[16] J. Wei, Y. Lei, H. Jia, J. Cheng, H. Hou, Z. Zheng, Dalton Trans. 43 (2014) 11333–11338.
[17] A.L. Linsebigler, G. Lu, J.T. Yates, Chem. Rev. 95 (1995) 735–758.
[18] Y. Tang, X. Hu, C. Liu, Phys. Chem. Chem. Phys. 16 (2014) 25321–25329.
[19] M.E. Rincón, M. Sánchez, J.R. García, J. Electrochem. Soc. 145 (1998) 3535–3544.
[20] P. Wang, B. Huang, X. Qin, X. Zhang, Y. Dai, J. Wei, M.-H. Whangbo, Angew. Chem. Int. Ed. 47 (2008) 7931–7933.
[21] A. Paracchino, V. Laporte, K. Sivula, M. Grätzel, E. Thimsen, Nat. Mater. 10 (2011) 456–461.
[22] A. Takai, P.V. Kamat, ACS Nano 5 (2011) 7369–7376.
[23] R. Chapman, P. Mulvaney, Chem. Phys. Lett. 349 (2001) 358–362.
[24] H. Choi, W.T. Chen, P.V. Kamat, ACS Nano 6 (2012) 4418–4427.

[25] C. Yu, G. Li, S. Kumar, K. Yang, R. Jin, Adv. Mater. 26 (2014) 892–898.
[26] X. Wang, H.-F. Wu, Q. Kuang, R.-B. Huang, Z.-X. Xie, L.-S. Zheng, Langmuir 26 (2009) 2774–2778.
[27] J. Roithová, D. Schröder, J. Am. Chem. Soc. 129 (2007) 15311–15318.
[28] X. Wang, S. Li, H. Yu, J. Yu, S. Liu, Chem. Eur. J. 17 (2011) 7777–7780.
[29] V. Subramanian, E.E. Wolf, P.V. Kamat, J. Am. Chem. Soc. 126 (2004) 4943–4950.
[30] O.A.D. Gallardo, R. Moiraghi, M.A. Macchione, J.A. Godoy, M.A. Perez, E.A. Coronado, V.A. Macagno, RSC Adv. 2 (2012) 2923–2929.
[31] T. Hirakawa, P.V. Kamat, J. Am. Chem. Soc. 127 (2005) 3928–3934.
[32] Z. Zhang, J.T. Yates, Chem. Rev. 112 (2012) 5520–5551.
[33] C.-W. Chen, P.-Y. Hsieh, H.-H. Chiang, C.-L. Lin, H.-M. Wu, C.-C. Wu, Appl. Phys. Lett. 83 (2003) 5127–5129.
[34] J.-M. Moon, J.-H. Bae, J.-A. Jeong, S.-W. Jeong, N.-J. Park, H.-K. Kim, J.-W. Kang, J.-J. Kim, M.-S. Yi, Appl. Phys. Lett. 90 (2007) 163516–163519.
[35] J.H. Hodak, I. Martini, G.V. Hartland, J. Phys. Chem. B 102 (1998) 6958–6967.
[36] R. Singh, B. Pal, J. Mol. Catal. A: Chem. 378 (2013) 246–254.
[37] Y. Dai, Y. Sun, J. Yao, D. Ling, Y. Wang, H. Long, X. Wang, B. Lin, T.H. Zeng, Y. Sun, J. Mater. Chem. A 2 (2014) 1060–1067.
[38] M.R. Hoffmann, S.T. Martin, W. Choi, D.W. Bahnemann, Chem. Rev. 95 (1995) 69–96.
[39] N.J. Bell, Y.H. Ng, A. Du, H. Coster, S.C. Smith, R. Amal, J. Phys. Chem. C 115 (2011) 6004–6009.